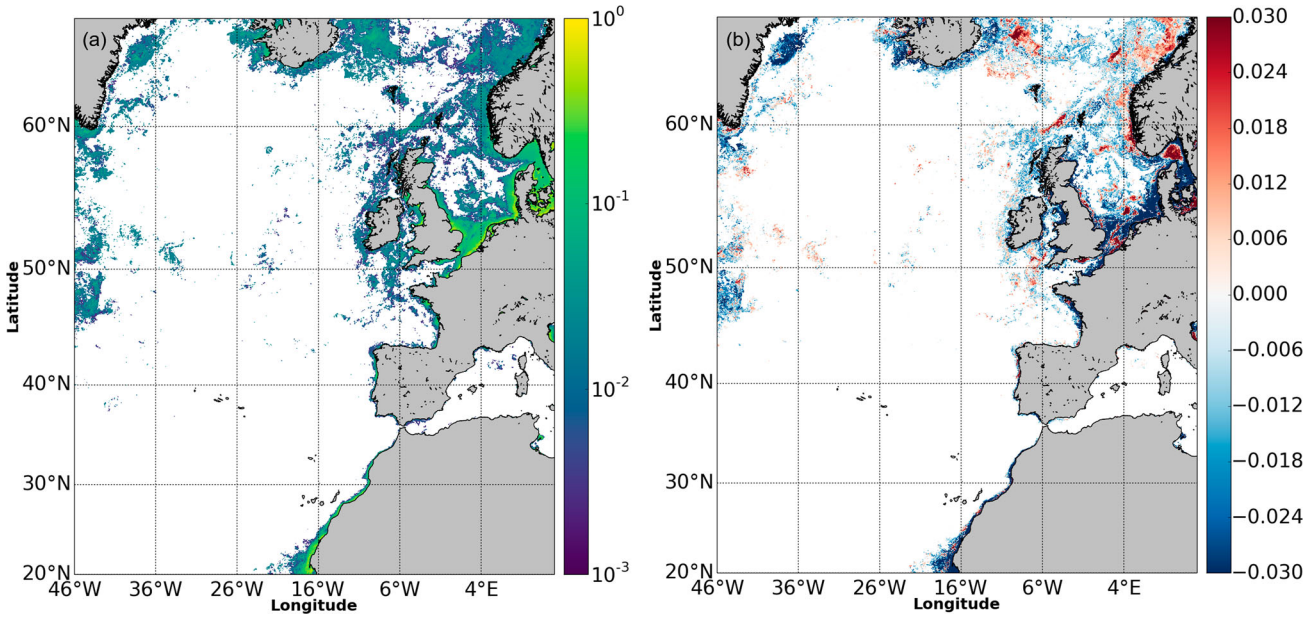

Figure 2.1.3. Regional 2018 mean diatom index (a) and regional 2018 diatom index anomaly (b) with respect to the 1997–2017 climatology of the diatom index, based on the CMEMS diatom fractional chlorophyll concentration product (product ref. 2.2.1).

value. The most important negative anomalies were detected in the coastal regions of the North Sea. A full time series analysis of the diatom index and corresponding indices for the other functional types and size classes is required to put this annual anomaly in the context of the decrease in diatom dominance predicted in the literature, as one of the consequences of climate change.

It has been predicted on the basis of models and observations that climate change can impact phytoplankton community structure, and that the distribution of diatoms in particular could be affected (Bopp et al. 2005; Cermeño et al. 2008; Marinov et al. 2010). The diatom products presented here offer a satellite-based tool to study spatial and temporal variations in diatom dynamics at high resolution in space and over long time scales. The time series of the climate-quality ocean-colour products is now 20 years long and growing, and the value of these products can only increase as the length of the time series grows. Ciavatta et al. (2018) have demonstrated that information on community structure of phytoplankton, when assimilated into ecosystem models, can help improve model performance.

Section 2.2: Primary production

Authors: Gianpiero Cossarini, Marine Bretagnon, Valeria Di Biagio, Odile Fanton d'Andon, Philippe Garnesson, Antoine Mangin, Cosimo Solidoro

Statement of main outcome: Primary production is at the base of the marine food web and an important factor in the Earth's carbon cycle. In this study, we used a remote sensing algorithm to estimate the reference state and trend of the global ocean primary production. Given the availability of the CMEMS reanalysis for the Mediterranean Sea, we focus on this marginal sea providing a merged estimate and its uncertainty. Spatial variability is high in the global ocean with the most productive areas located in the Arctic and coastal regions. Temporally, the seasonal cycle is an important component of the productivity of marine ecosystems. The most productive period is observed during summer time (austral or boreal) for each Hemisphere globally and also for the Mediterranean Sea regionally. A small but significant decrease in primary production has been observed over the past 20 years for the global ocean, whereas a small but significant increase has been observed in the Mediterranean Sea. High interannual variability is also reported and possibly triggered by year-to-year changes in physical forcing, such as the strength of the vertical mixing.

Product used:

Ref. No.	Product name and type	Documentation
2.2.1	MEDSEA_REANALYSIS_BIO_006_008	PUM: http://marine.copernicus.eu/documents/PUM/CMEMS-MED-PUM-006-008.pdf QUID: http://marine.copernicus.eu/documents/QUID/CMEMS-MED-QUID-006-008.pdf
2.2.2	SST_GLO_SST_L4_REP_OBSERVATIONS_010_011 SST_GLO_SST_L4_NRT_OBSERVATIONS_010_001	PUM: http://marine.copernicus.eu/documents/PUM/CMEMS-OSI-PUM-010-011.pdf QUID: http://marine.copernic

(*Continued*)

Continued.

Ref. No.	Product name and type	Documentation
		us.eu/documents/QUID/CMEMS-OSI-QUID-010-011.pdf
2.2.3	OCEANCOLOUR_GLO_OPTICS_L4_REP_OBSERVATIONS_009_081	PUM: http://marine.copernicus.eu/documents/PUM/CMEMS-OC-PUM-009-ALL.pdf QUID: http://marine.copernicus.eu/documents/QUID/CMEMS-OC-QUID-009-030-032-033-037-081-082-083-085-086-098.pdf
2.2.4	Climatology of the Mixed Layer depth (http://www.ifremer.fr/cerweb/deboyer/mld/Surface_Mixed_Layer_Depth.php)	http://www.ifremer.fr/cerweb/deboyer/mld/Data_Description.php
2.2.5	OCEANCOLOUR_GLO_CHL_L4_REP_OBSERVATIONS_009_082 OCEANCOLOUR_GLO_CHL_L4_NRT_OBSERVATIONS_009_033	PUM: http://resources.marine.copernicus.eu/documents/PUM/CMEMS-OC-PUM-009-ALL.pdf QUID: http://resources.marine.copernicus.eu/documents/QUID/CMEMS-OC-QUID-009-030-032-033-037-081-082-083-085-086-098.pdf
2.2.6	MEDSEA_REANALYSIS_PHY_006_004	PUM: http://marine.copernicus.eu/documents/PUM/CMEMS-MED-PUM-006-004.pdf QUID: http://marine.copernicus.eu/documents/QUID/CMEMS-MED-QUID-006-004.pdf

2.2.1. Introduction

Marine primary production is a fundamental component of marine ecosystem functioning and related ecosystem services (Hattam et al. 2015; Watson et al. 2015). It is at the base of oceanic food-webs and contributes to atmospheric CO_2 sequestration through CO_2 fixation and subsequent organic carbon sink (Siegel et al. 2016; Morrow et al. 2018). During daylight phytoplankton fixes carbon and nutrients through biological conversion of solar radiation (i.e. photosynthesis) and produces oxygen and organic matter (Falkowski 2003). Primary production drives the biological carbon pump and affects the amount of atmospheric carbon potentially sequestrated by the ocean, which highlights one of the roles of the ocean in the global carbon cycle (Falkowski et al. 1998; Henson et al. 2012; Le Quéré et al. 2018). In addition, primary production is a proxy of the potentially available food for higher trophic levels, thus serving as a potential indicator for the fishery management strategies, such as the Common Fisheries Policy EU directive (Chassot et al. 2010). Furthermore, primary production can be an important indicator for descriptors of the EC Marine Strategy Framework Directive such as D4 'Food Web' (Lynam et al. 2016) and D5 'Eutrophication' (OPEC project, D2.8, opec-marine.eu). Marine primary production varies generally between 440 $mgC.m^{-2}.d^{-1}$ in the open ocean and oligotrophic areas, and 1400 $mgC.m^{-2}.d^{-1}$ in the most productive waters, such as upwelling systems (Chavez et al. 2011). The spatial distribution of primary production is generally linked to nutrients supply and its temporal dynamics usually follow a seasonal cycle, constrained by the seasonality of solar radiation, nutrient supply and stability of the water column (Longhust 1995). At interannual or longer timescales, oceanic primary production is essentially a function of the physical parameter variability (Chavez et al. 2011). Consistently with the Ocean State Report guidelines, the aim of this study is to provide the reference state (1999–2014 period), the trend analysis (1999–2018) and the 2018 anomalies of primary production in the global ocean, with a focus on some European seas (i.e. North Atlantic Sea, Baltic Sea and Mediterranean Sea), using a satellite archive. Satellite estimates of primary production are merged with modelling results available for the Mediterranean domain, which is often considered as a 'miniature ocean' (e.g. Béthoux and Gentili 1999; Lejeusne et al. 2010), with a western basin about 50% more productive than the eastern basin (Moutin and Raimbault 2002). The Mediterranean Sea represents a sensible region to study environmental forcing and climate change impacts on primary production. Here we provide some insights on the influence of winter vertical mixing, nutrient supply and solar radiation on the ecosystem productivity. Finally, this study provides insights in similarities and discrepancies between the two approaches (i.e. modelling and satellite), addressing the uncertainty associated to the estimation of this important ecosystem functioning indicator.

2.2.2. Method

Photosynthesis occurs in the euphotic layer, generally characterised by a homogeneous production profile in case of mixing conditions and by a subsurface maximum in case of stratification. Estimates of the marine ecosystem primary production are usually integrated vertically over the productive layer. In the present study the vertically integrated primary production at global and regional scales is assessed through combining satellite-derived datasets of chlorophyll-*a* and model reanalysis over the past 20 years (1999–2018). Satellite results are integrated over the productive layer (i.e. 1.5 times the euphotic depth), while the Mediterranean Sea model output is integrated over 0–200 m depth, which safely covers the whole productive layer.

At the global scale, primary production is estimated with the Antoine and Morel satellite algorithm (Antoine and Morel 1996) using the Copernicus Marine Environment Monitoring Service (CMEMS) monthly merged ocean colour product (chlorophyll-*a* and photosynthetic

active radiation) from CMEMS (cf. 2.2.3 in the product table) with a spatial resolution of 4 km. Monthly averaged sea surface temperature comes from the OSTIA product from CMEMS, at 1/12° spatial resolution (Donlon et al. 2012, cf. 2.2.2 in the product table), and it is linearly interpolated to 4km.

In the Mediterranean Sea, vertically integrated primary production is estimated by averaging the aforementioned product (cf. 2.2.3) with the results of the CMEMS Mediterranean reanalysis (cf. 2.2.1). To estimate the uncertainties associated to the merged product, we computed the signal-to-noise ratio, as the ratio between mean and standard deviation of the monthly maps of primary production from satellite data and modelling output. The difference between satellite and model values is estimated as the reciprocal of this ratio and it is equal to 20% on average.

The CMEMS reanalysis is provided by the coupled physical-biogeochemical reanalysis model NEMO3.4 (Simoncelli et al. 2014) and OGSTM-BFM (Lazzari et al. 2012, 2016; Canu et al. 2015; Cossarini et al. 2015, Teruzzi et al. 2016) with data assimilation of temperature and salinity vertical profiles and satellite sea level anomaly (Dobricic and Pinardi 2008), and surface chlorophyll concentration (Teruzzi et al. 2014, 2018). The horizontal grid resolution of the model is 1/16° (ca. 6–7 km) and the unevenly spaced vertical levels are 72. The modelled net primary production is computed as the difference between the gross primary production and the phytoplankton respiration (Lazzari et al. 2012; Vichi et al. 2015). Following Geider et al. (1997), the Biogeochemical Flux Model (BFM) parameterisation describes the gross primary production in terms of photosynthetic available radiation (PAR), temperature, carbon quota in phytoplankton cells, chlorophyll content per unit of carbon biomass (i.e. chlorophyll dynamics is decoupled from uptake and growth dynamics and includes synthesis, degradation and photo adaptation), and nutrient (nitrogen, phosphorus, silicon) availability. Respiration includes both active (i.e. coupled to the production) and rest (i.e. correlated to the phytoplankton biomass) terms.

2.2.3. Reference state and seasonal cycle of primary production

At the global scale, primary production is on average of 57.6 GtC.yr^{-1}, in line with previous satellite estimations (31.2–72.8 GtC.yr^{-1}; Carr et al. 2006; Westberry et al. 2008). The highest values (>800 mgC.m^{-2}.d^{-1}) are observed in coastal regions and in upwelling areas (Figure 2.2.1(a)), where nutrients are injected in the surface layer. In contrast, the lowest values (<200 mgC.m^{-2}.d^{-1}) are observed in the open ocean, in the oligotrophic gyres, where nutrient concentration is low (Perruche et al. 2018). Note that due to lack of light, the high latitudes (> 60°) are not covered by satellite observations. However, the North Atlantic is more productive than the surrounding area, with values up to 700 mgC.m^{-2}.d^{-1}. The high productivity in the subpolar north Atlantic is mainly due to the deep winter mixing, which brings an important amount of nutrients into the surface layer. In the Gulf Stream area, the high productivity is explained by the meso- and submesoscale activity (Lévy et al. 2001, 2012).

In the Mediterranean Sea, primary production (Figure 2.2.1(b)) shows a west-to-east decreasing gradient with the highest values in the Alboran Sea. Local higher maxima are found in coastal areas influenced by river input, such as in Aegean and Adriatic Seas (Salon et al. 2019). These results are consistent with previous basin wide studies (Bosc et al. 2004; Lazzari et al. 2012) and with the general view of increasing west–east oligotrophication gradient (Siokou-Frangou et al. 2010). The overall mean value of primary production equals to 385 mgC.m^{-2}.d^{-1}, but large differences are observed between the western and eastern basins. The mean values in the western and the eastern (excluding the marginal seas) areas are 488 and 306 mgC.m^{-2}.d^{-1}, respectively, which fall between previous estimations (i.e. 216–526 mgC.m^{-2}.d^{-1} for the western basin and 189–427 mgC.m^{-2}.d^{-1} for the eastern basin; Bosc et al. 2004; Uitz et al. 2012). Satellite and model estimates are quite consistent, with an average difference of 20%. We observe differences greater than 33% (i.e. with a signal-to-noise ratio lower than 3) for 6 or more months only in few limited areas (e.g. mainly coastal and central Levantine areas, Figure 2.2.1(b)).

Primary production is driven by the seasonal cycle of stability of the water column, illumination and nutrient supply (Longhust 1995). Distinctive seasonal regimes can be recognisable for biogeographical regions of the global oceans (Longhust 1995; Ducklow 2003). For sake of brevity and without claim of exhaustiveness, we provided an essential overview of the seasonal cycle of primary production in global ocean and selected European seas (Figure 2.2.2). In the global ocean (Figure 2.2.2(a)) the seasonal cycle is characterised by two peaks and two minima and a quite smooth temporal variability, since it takes into account the north and south hemispheres and the presence of wide oligotrophic areas with weak seasonality. The most productive season occurs in boreal summer, with a peak in June of about 430 mgC m^{-2} d^{-1}. The second maximal production occurs in austral summer, between December and January, and reach a rate of about 380 mgC m^{-2} d^{-1}. In the Baltic Sea, the increasing of primary production as the

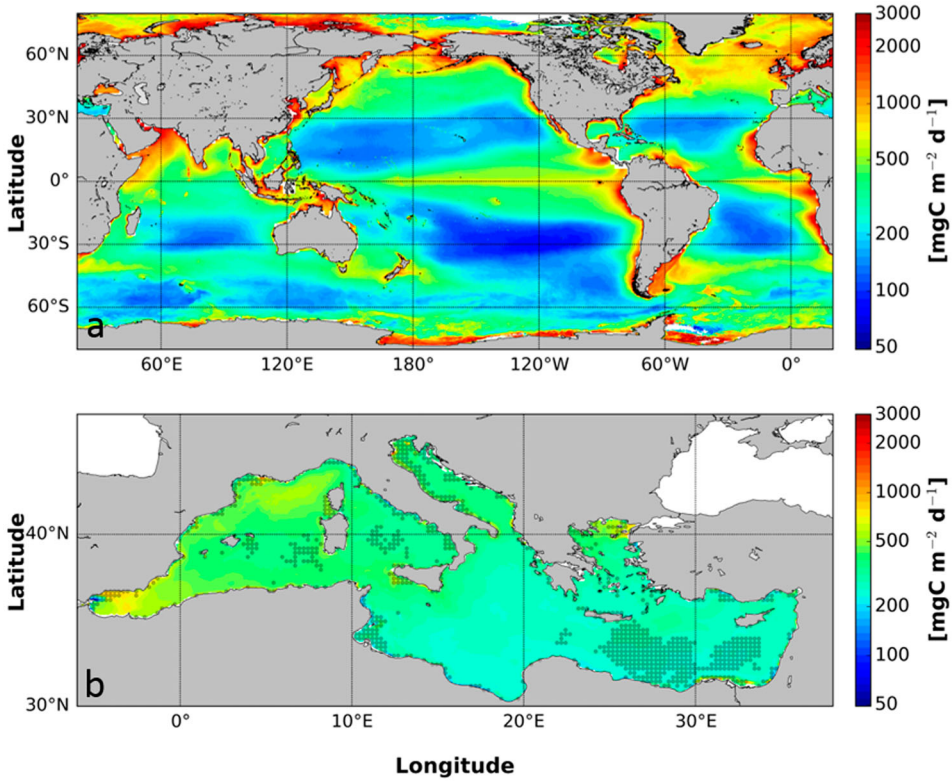

Figure 2.2.1. Map of 1999–2014 climatology of vertically integrated primary production (1999–2014 average) at global scale (a) and in the Mediterranean Sea (b). The global map is provided by satellite archive, whereas the Mediterranean map is the merged product (average of the satellite and model maps) reported to the 1/16° resolution. The areas with signal-to-noise ratio lower than 3 for 6 or more months are marked by the black dots. (Products 2.2.5 and cf.2.2.1).

consequence of the summer bloom is the strongest compared to the other marginal seas here considered (Figure 2.2.2(a,b)). Indeed, primary production in summer (up to 3100 mgC m^{-2} d^{-1} in August) is almost three times higher than winter values (down to 1300 mgC m^{-2} d^{-1} in February) . Also, due to the winter night, primary production can not be monitored from remote sensing between November and January. In this region, primary production appears to be limited by the light availability and the sea ice cover. The North Atlantic seasonal cycle (Figure 2.2.2(a)) is characterised by summer maxima, when the highest primary production values (up to 1300 mgC m^{-2} d^{-1} in June) are coincident with the maximum of the light availability.

In the Mediterranean Sea, the seasonal cycle of primary production presents two significant increases at a basin scale (Figure 2.2.2(b)). First, a rapid increase in primary production occurs in March (about 400 mgC m^{-2} d^{-1}) due to late winter-early spring phytoplankton blooms sustained by winter vertical mixing that supplies nutrients into the surface layer (Lazzari et al. 2012). Second, a year maximum occurs during summer, concurrent with the seasonal variation of light availability for the photosynthesis (Antoine et al. 1995; Bosc et al. 2004). Note that the intensity of the seasonal cycle is higher than for the oceans above mentioned. Indeed, while production in summer is twice as high as production in winter for the Mediterranean Sea, production increases only about 40% between winter and summer for the global ocean. The Mediterranean Sea can be subdivided in two parts linked to the well-known oligotrophic west-to-eastern gradients (Moutin and Raimbault 2002; Siokou-Frangou et al. 2010). Our results confirm that the western part (i.e. from 5°W to the Sicily channel at 12°E in Figure 2.2.1) is about 44% more productive than the eastern part and has a less smooth seasonal pattern (Figure 2.2.2(b)). Hovmöller diagrams of Figure 2.2.2(c,d) report the monthly means along the water column and shed some light on the two different mechanisms driving the different regimes in the Mediterranean basins. In the western basin the increase due to the late winter-early spring primary production is restricted to the upper layer (Figure 2.2.2(c)) and is due to intense blooms at surface, where nutrients are supplied into the shallow euphotic layer by the winter mixing (Lòpez-Jurado et al. 2005; Schroeder et al. 2008; Volpe et al. 2012; Mayot et al. 2017). The surface winter-early spring bloom accounts for up to 40% of the

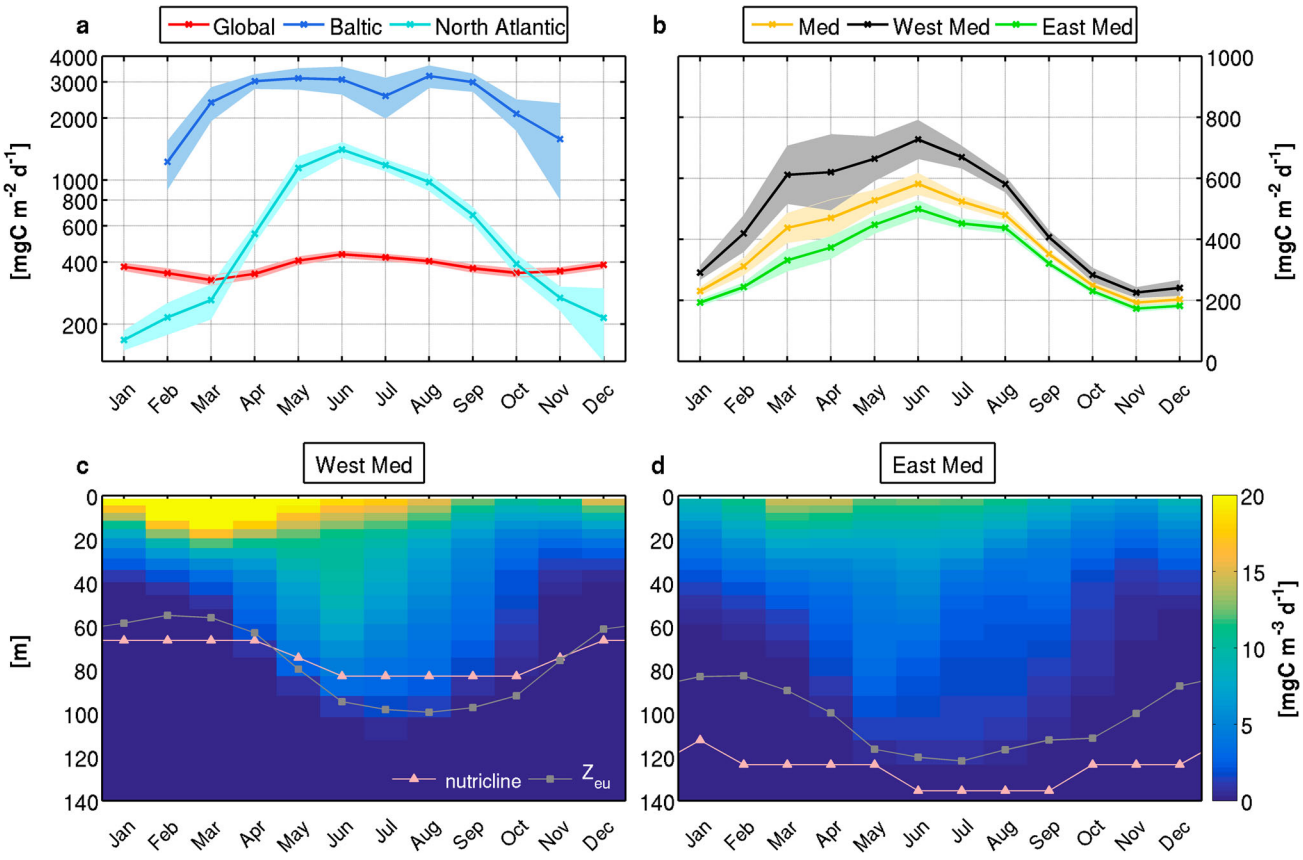

Figure 2.2.2. (a) Average seasonal cycle of primary production calculated in global ocean (red line), Baltic Sea (blue line) and North Atlantic Sea (cyan line) from the satellite archive in the reference period (1999–2014). (b) Average seasonal cycle of primary production calculated in Mediterranean Sea (yellow line) and in the western basin (black line) and eastern basin (green line) from the merged product in the reference period (1999–2014); envelopes in (a) and (b) represent the standard deviation as inter-annual variability. Hovmöller diagrams of mean monthly volumetric primary production [mgC m^{-3} d^{-1}] for the western (c) and eastern (d, excluding marginal seas) Mediterranean basins, computed from the reanalysis archive in the reference period (1999–2014); pink triangles represent the mean monthly nutricline, computed as the depth which separates levels of values of nitrate concentration higher and lower than 1 mmol m^{-3}, on the 1999–2014 reanalysis archive; grey squares represent the monthly mean euphotic depth (Zeu), as the depth at which the modelled PAR is 1% of its surface value, according to BFM formulation (Lazzari et al. 2012). (Products 2.2.5 and 2.2.1).

mean annual primary production. Beside the late winter-early spring surface increase, the second highest contribution to the annual primary production values are observed in the subsurface layer in late spring and summer (Figure 2.2.2(c,d)). The eastern basin has generally lower values of volumetric primary production, associated to a deeper nutricline (120 m depth in winter, Figure 2.2.2(d)) with respect to the western basin (70 m, Figure 2.2.2(c)), which makes less effective the upward nutrient supply by winter mixing. Nevertheless, the depth of the euphotic layer in the eastern basin is greater than that of the western basin (120 and 100 m of maximum depth in summer, respectively) and substantial productivity, up to 15 mgC.m^{-3}.d^{-1}, can be found down to 120–130 meters depth in July and August (Figure 2.2.2(d)). The thickness of the productive layer follows the onset of the deep chlorophyll maximum, which is common in the subsurface layer of the oligotrophic stratified waters of the Mediterranean Sea (Barbieux et al. 2019) and is found at greater depth in the eastern Mediterranean basin than in the western basin (Lavigne et al. 2015; Cossarini et al. 2019).

2.2.4. Trend and interannual variability

Following the Vantrepotte and Mélin census I methods (Vantrepotte and Mélin 2009), the time series of the spatially averaged monthly primary production is decomposed into the seasonal component (shown in Figure 2.2.2) and an anomaly, from which the linear trend is estimated (Figure 2.2.3). Over the archive 1999–2018, the time series of primary production highlight the interannual variability with respect to the mean seasonal component for the global ocean and the European regional seas (Figure 2.2.3(a–f)). Indeed, the first years of the time series (Figure 2.2.3(a)) exhibit higher values, which might be explained by a La Niña event, as it impacts upwelling and therefore nutrient

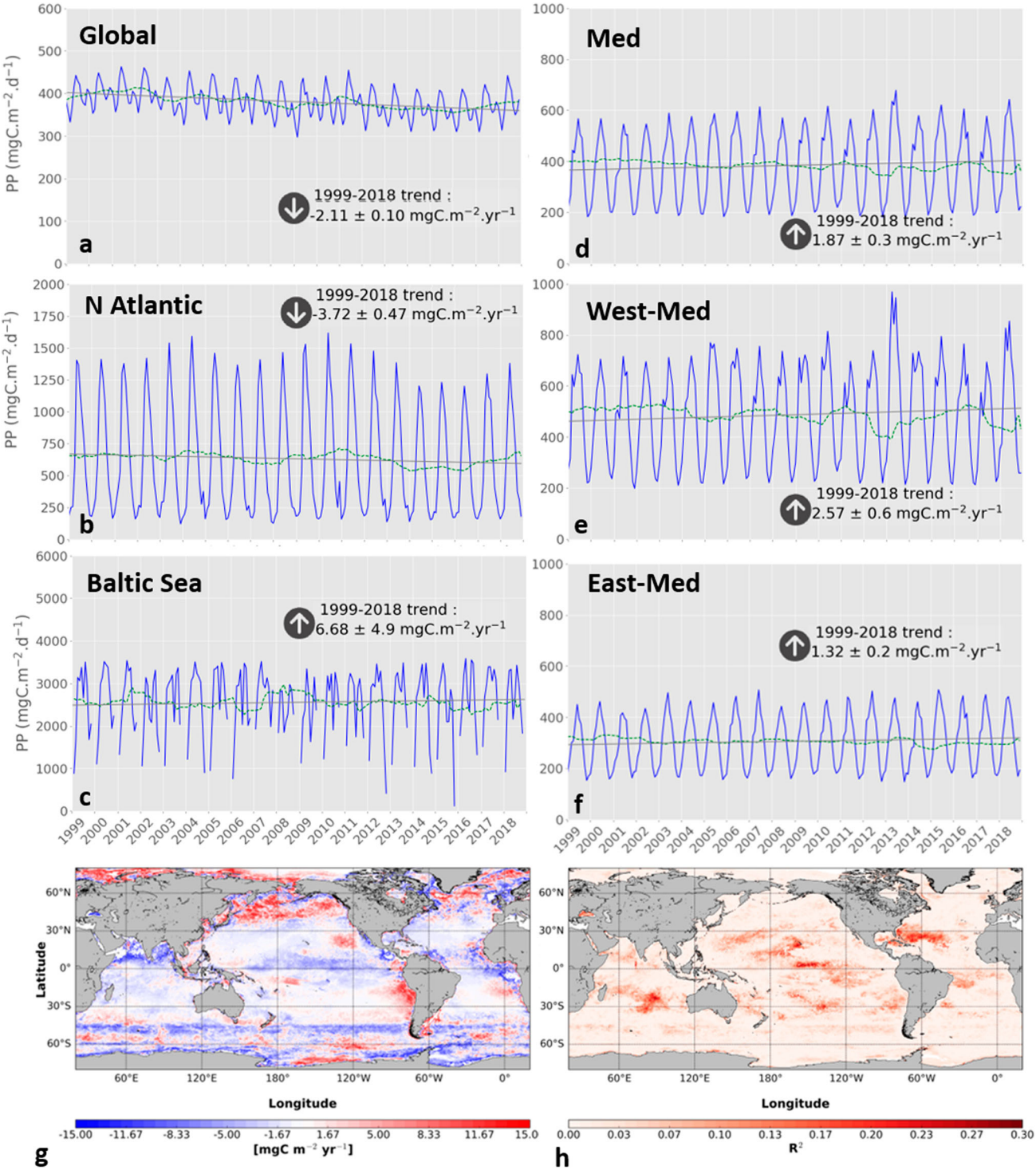

Figure 2.2.3. Primary production time series over the 1999–2018 period, for the satellite archive in global ocean (a), North Atlantic Sea (b) Baltic Sea (c), and for the merged product in Mediterranean Sea (d), Western Mediterranean Sea (e), Eastern Mediterranean Sea (f). Each plot reports the monthly time series (blue line), the time series obtained by subtracting the seasonal and residual components (green line) and the trend (grey line), which is estimated following the Vantrepotte and Mélin census I method (Vantrepotte and Mélin 2009). For each basin, the arrow indicates the sign of the trend, which is reported in terms of annual variation and standard error. Panel (g) presents the map of the trend of primary production at the global scale, computed at each pixel except in Mediterranean Sea from the satellite archive and panel (h) the coefficient of determination for the trend estimated at each pixel. (Product 2.2.5 for the global ocean, and 2.2.5 and 2.2.1 for the Mediterranean Sea).

availability (Behrenfeld et al. 2006). In addition to El Niño Southern Oscillation variations, other climate indexes (e.g. Pacific Decadal Oscillation, North Atlantic Oscillation) may contribute to explain the interannual variability (Rousseaux and Gregg 2014). Indeed, the evolution of primary production anomalies (after seasonal cycle removal) in the North Atlantic Sea appears to be negatively correlated with NAO phases (not shown). Generally, periods of positive anomalies of at least 5 months long are associated with negative NAO and vice versa. This is particularly evident during some events: in summer 2013 (i.e. negative primary production anomaly and positive NAO) and in summer 2008 and 2010 (i.e. positive primary production anomalies and negative NAO).

Primary production decreases of 2.11 ± 0.10 $mgC.m^{-2}.yr^{-1}$ ($R^2 = 0.64$) at the global scale over the temporal archive (Figure 2.2.3(a)). The decline of primary production at the global scale can be explained by the warming of water column, which induces stratification (Von Schuckmann et al. 2019) and nutrient surface depletion. However, the decrease in primary production is not homogeneous and we observe a high spatial variability (Figure 2.2.3(g)), which is related to local environment conditions. For example, a positive trend of primary production is observed in the south Greenland area and it is related to the nutrient supply after sea ice melting (Bhatia et al. 2013; Hawkings et al. 2015; Lawson et al. 2014). Thinning and shortening of sea ice cover in the Baltic Sea (Tedesco et al. 2017) explains the positive, even if not significant, trend in the Baltic Sea (6.68 ± 4.9 $mgC.m^{-2}.yr^{-1}$, Figure 2.2.3 (c)). Conversely, primary production over the entire North Atlantic decreases of 3.72 ± 0.47 $mgC.m^{-2}.yr^{-1}$ ($R^2 = 0.25$). This decline in primary production appears to be related to the increasing stratification and the decreasing of upwelling favourable wind (Kwiatkowski et al. 2019). The increasing primary production off Greenland and the global decrease in the North Atlantic highlight the spatial and temporal variability in this region. In general, our trend map is in good agreement with chlorophyll trend estimated by Gregg et al. (2017), with both maps reporting, for instance, positive trends in the south east Pacific area, even if the coefficient of determination is relatively low for the considered archive.

A small positive and significant trend is estimated for the whole Mediterranean Sea over the period 1999–2018 (1.87 ± 0.3 mgC m^{-2} yr^{-1}, $p < .01$, Figure 2.2.3(d)), while the western basin displays a significant positive trend of about 2.57 ± 0.6 mgC m^{-2} yr^{-1} (Figure 2.2.3(e)). Our result in the western Mediterranean Sea is in agreement with the positive trend of chlorophyll detected in the same area by Salgado-Hernanz et al. (2019) who report an increase of the amplitude and duration of the phytoplankton growing period, on the 1999–2014 subset of Product 2.2.5. Different long term signals have been reported for other Mediterranean regions (e.g. negative or neutral) supporting the conclusion that environmental and climate forcings have local and complex impacts in the Mediterranean Sea (Salgado-Hernanz et al. 2019).

The Mediterranean time series (Figure 2.2.3(d)) displays also substantial interannual variability, which is larger than the trend signal (not shown). The fluctuations are higher in the western Mediterranean Sea than in the eastern basin (Figure 2.2.3(e,f)). This spatial heterogeneity is related to the different oceanographic characteristics of the two basins: generally stratified and oligotrophic the eastern basin and influenced by intense winter mixing and the presence of some frontal systems the western basin (Siokou-Frangou et al. 2010). Insights into the impact of interannual variability of the winter mixing on primary production anomalies are provided in Figure 2.2.4. The highest values of winter mixed layer depth are generally followed by positive anomalies of primary production (i.e. productivity higher than the average in 2006, 2010, 2013, 2014 and 2018; Figure 2.2.4). Indeed, the interannual variability of the winter-early spring primary productivity is pretty well explained by the late autumn–winter interannual variability of the winter deep mixing: the correlation between time series of November-February averages of mixed layer depth (data from cf. 2.2.6 in the product table) and January-May averages of primary production is 0.77, $p < .005$.

Strong interannual variability and a stepwise increase of the dense water formation in the north-western Mediterranean is reported starting from winter 1999 after a period of low convective activity during the 1990s (Somot et al. 2018). Increased number of winters with enhanced mixing in the most recent years can have impacted the nutrient supply in the euphotic layer determining the positive trend of primary production in the western basin (Kessouri et al. 2018).

2.2.5. The 2018 anomaly

At global scale, the anomalies for 2018 relative to the reference period 1999–2014 indicate a lower-than-average primary production in 2018, indeed the average of the 2018 anomaly map is about −17% (Figure 2.2.5(a). In the Gulf Stream area and along the North American coast, primary production anomalies are below the average. Lower-than-average primary production values in the Californian upwelling are potentially linked to the intensification of the wind drop-off, known to affect

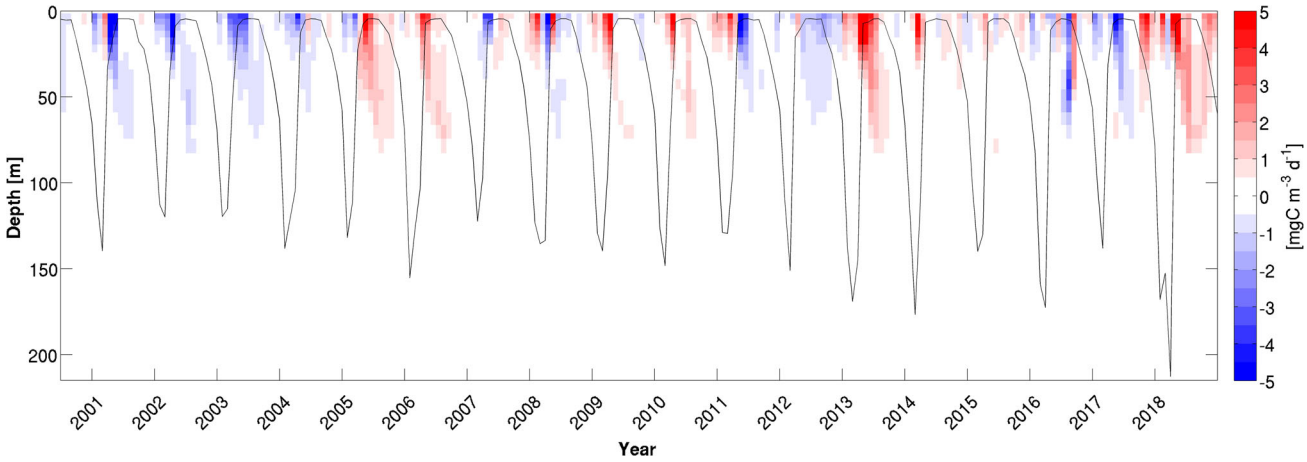

Figure 2.2.4. Time series of the monthly anomalies of the modelled primary production (product. 2.2.1) along the water column with respect to the 1999–2014 monthly means of Figure 2.2.2(c), and time series of mixed layer depth (black line) in the western part of the Mediterranean Sea (Product 2.2.6).

primary production in this region (Renault et al. 2016). Higher-than-average values (increasing productivity) are observed in the south subtropical Pacific. However, since the subtropical ocean is oligotrophic, a small increase in productivity can represent a relatively large positive anomaly.

In the Mediterranean Sea the anomalies for 2018 (Figure 2.2.5(b)) are generally positive in the western basin, consistently with the positive spring increase shown in the time series of anomalies (Figure 2.2.4). Intense vertical mixing in the autumn 2017-winter 2108 period (Figure 2.2.4) triggered a larger nutrient supply to the euphotic layer (as inferred from Figure 2.2.2(c)) and, thus, caused the positive anomaly in 2018. The eastern Mediterranean Sea is characterised by an almost balanced overall anomaly with no

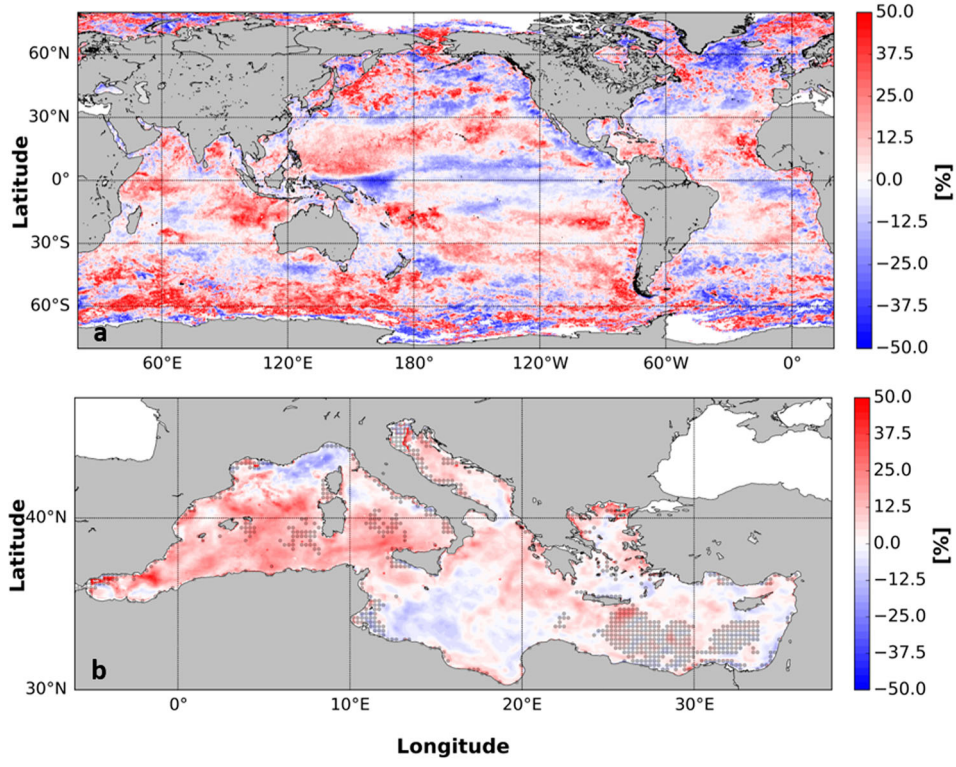

Figure 2.2.5. Map of the relative anomalies of 2018 with respect to the 1999–2014 reference state for the global ocean except Mediterranean Sea (a), estimated from satellite observation, and for the Mediterranean Sea (b), estimated from the merged product. (Products 2.2.5 and 2.2.1). The black dots area indicates the signal-to-noise ratio of the reference state map

particular spatial patterns. High positive anomalies in the northern Adriatic Sea and Northern Aegean Sea should be considered with caution since affected by low signal-to-noise ratios.

Section 2.3: Barrier layer thickness in the Pacific Ocean

Authors: Greiner Eric, Nathalie Verbrugge, Sophie Cravatte, Benoit Tranchant, Arnaud Valcarcel

Statement of main outcome: Barrier layers are ubiquitous in the tropical Pacific, with significant interannual, and decadal variations. Barrier layers act to trap the heat and motion in a thinner mixed layer. It is therefore an important indicator for subseasonal and seasonal forecasting (Madden-Julian Oscillations, El Nino, etc.). The 2018 anomaly is not very different from climatology. The barrier layer is generally thickening over 1993–2018 in the western Pacific and thinning in the central Pacific. Barrier layers may also be an indicator of water cycle changes. The barrier layer indicator could help to monitor these long-term changes and their impacts in near-surface stratification.

Products used:

Ref. No.	Product name & type	Documentation
2.3.1	Global Ocean Observation-based Products MULTIOBS_GLO_ PHY_REP_015_002	PUM: http://marine.copernicus.eu/documents/PUM/CMEMS-MOB-PUM-015-002.pdf QUID: http://marine.copernicus.eu/documents/QUID/CMEMS-MOB-QUID-015-002.pdf
2.3.2	Pacific Decadal Oscillation Index (NOAA)	http://research.jisao.washington.edu/pdo/
2.3.3	Southern Oscillation Index (JISAO)	https://www.cpc.ncep.noaa.gov/data/indices/soi
2.3.4	Global Ocean- CORA – In-situ Observations Yearly Delivery in Delayed Mode INSITU_GLO_TS_REP_ OBSERVATIONS_013_001_b	http://marine.copernicus.eu/documents/PUM/CMEMS-INS-PUM-013-001-b.pdf http://marine.copernicus.eu/documents/QUID/CMEMS-INS-QUID-013-001b.pdf

2.3.1. Introduction

The mixed layer depth is controlled by temperature stratification in most areas of the world ocean. This is not the case in the tropics, where salinity stratification near the surface plays a dominant role, creating barrier layers (de Boyer Montégut et al. 2007; Mignot et al. 2007). A barrier layer is a quasi uniform isothermal layer located above the top of the thermocline, separated from the surface mixed layer by salinity stratification. It isolates the mixed layer from the cooler waters below. Barrier layers in the tropical Pacific are quasi-permanent, formed by a mix of complex physical processes including rainfall freshening, advection, and stretching (e.g. Cronin et al. 2002). They act to trap momentum and heat in a layer shallower than it would be with temperature stratification alone, and inhibit cooling by turbulent mixing with underlying waters, inducing higher sea surface temperature (Bosc et al. 2009) and stronger eastward zonal jets potentially contributing to the eastward displacement of the Warm Pool. They have thus the potential to influence the ocean heat budget, the Madden Julian Oscillation, the tropical cyclones, and the development of El Nino events (Maes et al. 2002). Better tracking them, and their thickness is thus key for subseasonal to seasonal predictions (Zhao et al. 2014; Zhu et al. 2014).

Barrier layers thickness is computed as the difference between the isothermal layer depth and the mixed layer depth. It varies at different timescales. A weak seasonal cycle of barrier layers in the western tropical Pacific has been found related to the eastern extension of the Warm Pool, and to seasonal variations in precipitation (Mignot et al. 2007). Most of the variability in tropical Pacific barrier layer thickness is on interannual time scale (Ando and McPhaden 1997; Bosc et al. 2009). Liu et al. (2009) indicated that barrier layers are thinning (thickening) during El Niño (La Niña) west of 160°E due to the change in precipitation. The changes in barrier layers' position and thickness however depend on the flavor of El Nino (Wang and Liu 2016) and the SST anomalies location (i.e. emergence in the central or eastern Pacific).

At decadal and longer timescales, variations in barrier layer thickness are harder to detect due to a lack of sufficient high-vertical resolution data. The sea surface salinity and barrier layer thickness variations appear to be closely linked to the Pacific Decadal Oscillation (Delcroix et al. 2007; Wang and Xu 2018), and to shifts in precipitation areas. During positive phases of the Pacific Decadal Oscillation, surface salinity anomalies exhibit a pattern similar to that of El Nino Southern Oscillation, with a larger meridional extent: surface salinity is lower in the western-central equatorial Pacific and higher in the south and north-western Pacific. Patterns of barrier layer thickness anomalies are more complex: barrier layers are thicker in the central-eastern equatorial Pacific, and thinner (by around 15 m) in the far western Pacific and in the southwest (Wang and Xu 2018).

Terray et al. (2012) and Durack (2015) found that the Western Pacific is freshening, following the global water cycle intensification attributed to anthropogenic change. Deser et al. (2012) have shown that, in the atmosphere, the response to anthropogenic forcing is more detectable in surface temperature than in